Jikeikai Med J 2020 ; 67 : 29-42

Usefulness of 2-Dimensional Speckle Tracking Echocardiography and Diffusion Tensor Imaging for the Detection of Myocardial Fibrosis in a Rat Model of Right Ventricular Pressure Overload

Fumie KAWACHI[1], Junichi HATA[2], Sadataka KAWACHI[3], Hirotaka James OKANO[2], Hiroyuki IDA[1], Takashi URASHIMA[1], and Daishi HIRANO[1]

[1]*Department of Pediatrics, The Jikei University School of Medicine*
[2]*Division of Regenerative Medicine, The Jikei University School of Medicine*
[3]*Department of Pediatric Cardiology, Saitama Children's Medical Center*

ABSTRACT

Background : Two-dimensional speckle tracking echocardiography (2DSTE) has attracted a great deal of attention as an index that more acutely reflects a decrease in ventricular contractility than ejection fraction. Diffusion tensor imaging (DTI) is useful in the diagnosis of myocardial infarction, mainly in the left ventricle. This study aimed to investigate whether 2DSTE and DTI could be used to predict right ventricular (RV) myocardial fibrosis.

Methods : Five-week-old Sprague Dawley rats were randomly divided into 2 groups : a pulmonary artery banding group and a sham group ($n = 10$ for both). The rats were killed after echocardiography and cardiac catheterization at 4 weeks postoperatively and underwent DTI and histological analysis.

Results : The pulmonary artery banding group showed significant RV fibrosis compared to the sham group, and there was a significant negative correlation between the RV longitudinal strain score and fibrosis (Spearman's $\rho = -0.42$, $P < 0.01$). Moreover, $\lambda 1$ showed a significant negative correlation with RV myocardial fibrosis based on the diffusion eigenvalues ($\lambda 1$, 2, 3) and fractional anisotropy ($\rho = -0.79$, $P = 0.036$). In addition, the number of myocardial fibers depicted on fiber tractography decreased as fibrosis increased in all sagittal, coronal, and lateral sections.

Conclusions : This study demonstrated the potential usefulness of 2DSTE and DTI as noninvasive options for the early diagnosis of RV fibrosis.

(Jikeikai Med J 2020 ; 67 : 29-42)

Key words : Right ventricular fibrosis, 2-dimensional Speckle tracking echocardiography, diffusion tensor imaging, fiber tractography

BACKGROUND

Right ventricular (RV) pressure overload is a common clinical feature of pediatric cardiology which results from various congenital conditions and procedures, including pulmonary valve stenosis, pulmonary artery (PA) stenosis after tetralogy of Fallot repair, and PA banding (PAB) for pulmonary overcirculation. Accurately assessing the function of the RV is difficult because of its anatomically and functionally complex form. A pressure-loaded RV eventually

Received : August 31, 2020 / Accepted : November 9, 2020
河内　文江，畑　　純一，河内　貞貴，岡野ジェイムス洋尚，井田　博幸，浦島　　崇，平野　大志
Mailing address : Daishi HIRANO, Department of Pediatrics, The Jikei University School of Medicine, 3-25-8 Nishi-Shimbashi, Minato-ku, Tokyo 105-8461, Japan.
E-mail : bqx1976@hotmail.com

becomes enlarged and, eventually, fibrotic. The degree of fibrosis affects the long-term prognosis of RV function. Thus, the early diagnosis of RV myocardial fibrosis by noninvasive means and timely pressure load release are vital. However, owing to the complex form of the RV, the normal structure of the RV is poorly understood, and the distribution of myocardial fibrosis within the pressure-loaded RV is also unclear. Furthermore, the complex form of the RV causes its traditional function to be inadequately assessed ; therefore, RV myocardial fibrosis is challenging to diagnose[1-3].

Two-dimensional Speckle tracking echocardiography (2DSTE) is an technique that might be used to measure strain values in arbitrary regions independent of the angle and has attracted a great deal of attention as a functional evaluation tool for both the left ventricle (LV) and the RV[4-6]. Because cardiac function at the site of myocardial fibrosis is impaired, we hypothesized that 2DSTE can be used to locally diagnose RV myocardial fibrosis after PAB.

Furthermore, we focused on diffusion tensor imaging (DTI), which is a noninvasive technique similar to echocardiography. This method expresses the strength and direction diffusion anisotropy information by fitting it to a 3-dimensional (3D) elliptical sphere (consisting of 3 basis vectors) called a tensor[7]. Because diffusion anisotropy can be quantified by tensor analysis, we postulated that the extent of RV myocardial fibrosis can also be quantified. Moreover, the anisotropy is weakened when the myocardial alignment is perturbed, such as in the infarcted foci of myocardial infarction, and the fractional anisotropy (FA) value approximates 0[8-10]. We hypothesized that, similar to myocardial infarction, RV myocardial fibrosis would also result in perturbations in the myocardial alignment, thereby leading to reduced anisotropy and diffusion coefficients in 3 directions (λ1, 2, and 3).

Therefore, this study aimed to demonstrate the potential for early diagnosis of RV myocardial fibrosis using 2 noninvasive measures : 2DSTE and DTI.

METHODS

Experimental protocol

Five-week-old Sprague Dawley rats that weighed 170 to 200 g (Sankyo Labo Service Corporation, Inc. ; Tokyo ; Japan) were randomly assigned to the PAB group or the sham group (n = 10 for both ; Fig. 1). Animals were anesthetized with isoflurane inhalation, intubated (18-G Angiocath catheter ; Nippon Becton Dickinson Co. Ltd., Tokyo, Japan), and maintained on 2% isoflurane by means of a small animal ventilator (Harvard Apparatus, Holliston, MA, USA). The ventilator was set at 10 μl/g of the full tidal volume and 100 breaths/minute. In the sham group, a left-side thoracotomy was performed between the fourth and fifth ribs, and the thymus gland was resected. In the PAB group, thoracotomy was performed in a similar way. Subsequently, using a 20-G catheter (1.88 mm in external diameter, Angiocath) as a guide, we ligated the main PA twice with a 4-0 silk suture just enough to induce mild RV enlargement. The first main PA ligation was performed softly, and the second ligation

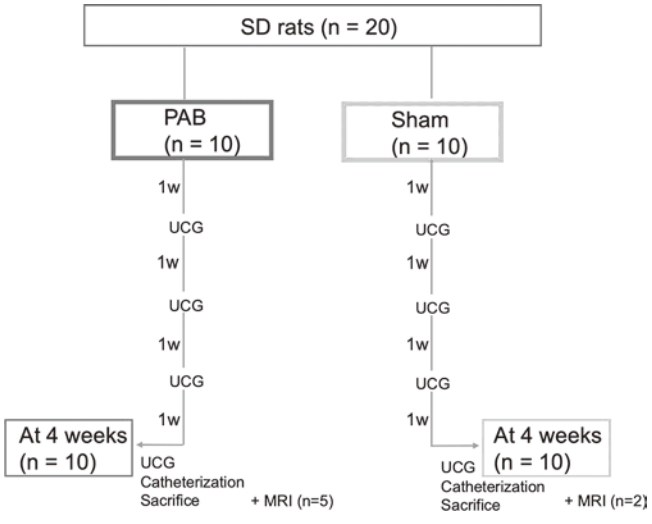

Fig. 1. Study protocol. UCG, ultrasound cardiography.

was performed so that it caused mild macroscopic RV hypertrophy but no RV dysfunction. We performed echocardiography after the chest had been closed, confirmed that tricuspid regurgitation (TR) was trivial, and noted no decrease in the RVFAC. Before closure, cardiac function, pneumothorax, and hemorrhage were evaluated in all rats, which were extubated after the return of spontaneous respiration.

A PAB flow ≤ 2.5 m/s was not observed with echocardiography in the PAB group 1 week postoperatively. After echocardiography and cardiac catheterization 4 weeks postoperatively, the rats were killed with pentobarbital. The entire heart was removed, the heart weight was measured, and histological analysis was performed. Seven of the removed hearts (2 in the sham group and 5 in the PAB group) underwent DTI before histological examination.

All rats were kept at 22°C ± 2°C under a 12-hours light/12-hours dark cycle, and all experiments were performed according to the study protocol. This study was performed after being approved by The Jikei University Institutional Animal Care and Use Committee (No. 2016-093C1).

Echocardiography

Echocardiography was performed with the Vivid E9 ultrasound system (GE Healthcare, Chicago, IL, USA) under inhalation sedation with 1.5% isoflurane. The variables measured were as follows : estimated RV pressure (RVp), RV fractional area change (FAC) in the 4-chamber view, LV ejection fraction (LVEF), tricuspid-to-mitral valve ratio (TV/MV), tricuspid annular plane systolic excursion (TAPSE), RV Tei index, heart rate (HR), and cardiac output (CO). The RVp was calculated with the formula RVp = right atrial pressure (RAp) + RV-PA pressure gradient, where an RAp of 5 mm Hg was assumed in all rats, and the simplified Bernoulli equation ($4 \times v^2$) was used for the RV-PA pressure gradient. The LVEF was measured in a single plane via the modified Simpson's method.

The 2DSTE analysis was performed with the Vivid E9 system and the dedicated software EchoPAC (version 112 ; GE Healthcare). The heart was divided into 4 segments : global RV, which included the interventricular septum (IVS) ; RV free wall ; global LV, which included the IVS ; and LV without the IVS. For each segment, longitudinal, circumferential, and radial strain measurements were recorded. For all samples the frame rate was 180 to 185 per second, and the HR was 352 ± 42 bpm.

Cardiac catheterization

Cardiac catheterization studies were performed with 2% isoflurane sedation and assisted ventilation before the rats were killed 4 weeks after the procedure. The LV pressure and RVp were measured with Mikro-Tip catheters (SPR-320NR, 2F ; Millar Instruments, Houston, TX, USA) that were inserted into the LV and RV via the left carotid artery and right jugular vein, respectively. Pressure data were analyzed with the Chart program supplied with the PowerLab system (AD Instruments, Colorado Springs, CO, USA), which calculated mean pressures for at least 10 consecutive beats. The correlation between mean RVp and echocardiographically estimated RVp was examined and confirmed.

Histopathologic examination

So that the the extent and distribution of fibrosis could be determined, the rats were killed with pentobarbital, and the entire heart was removed, weighed, and fixed in 10% formalin. After 4 weeks of fixation, the heart was divided evenly into 4 sections in a transverse direction from the RV outflow tract to the apex (Fig. 2a). After DTI, specimens were fixed in 10% formalin for 2 weeks and then histologically examined. Masson's trichrome staining was performed to evaluate the muscle fibers. To calculate the fibrosis rate (% ; Fig. 2b) in each region, we used the Image-Pro Premier 9.2 image analysis software program (Media Cybernetics, Washington, WA, USA) to determine the ratio of the fibrotic area to total area. Slice 1 was used to estimate the fibrosis rate at the RV outflow tract (RVOT) level ; the global RV, RV free wall, global LV, LV without IVS, and IVS fibrosis rates were determined from each corresponding area on slices 2 to 4 ; and the means of 3 slices were calculated.

Magnetic resonance imaging

Sample processing

After cardiac catheterization, the heart, which was fixed for 2 weeks in diastole, was wrapped in a sponge, soaked in fluorine solution (Sumitomo 3M Ltd., Tokyo, Japan), and placed in a plastic container. With magnetic resonance imaging (MRI), no signal from the heart was exhibit-

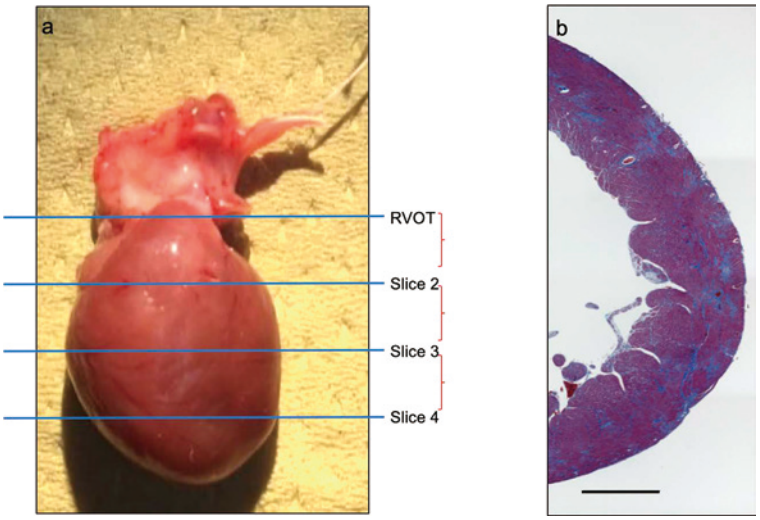

Fig. 2. Histological evaluation of fibrosis. (a) The image source is an isolated heart. The whole heart was dissected into 4 slices of equal thickness from the base to the apex. Slice 1 represented the RVOT. Slices 2 and 3 contained the global RV, RV free wall, global LV, LV without IVS, and IVS regions. (b) The image source is a strip preparation. Example of RV free wall region in slice 2 stained with Masson's trichrome (× 100). Fibrosis rate (%) = fibrotic area : blue / (myocardial area : red + fibrotic area) × 100. Scale bar = 1 mm. RVOT, right ventricular outflow tract ; RV, right ventricle ; LV, left ventricle ; IVS, interventricular septum.

ed.

Samples of the heart were also degassed under vacuum to reduce air artifacts. DTI was performed in 7 cases (2 in the sham group without RV fibrosis after echocardiography at 4 weeks postoperatively, 3 in the PAB group with a moderate pressure load of 40 ≤ RVp ≤ 70 mm Hg, and another 2 in the PAB group with RVp > 70 mm Hg).

Image acquisition

Images were acquired with a 9.4-T preclinical MRI scanner (BioSpec 94/30 ; Bruker Corp., Billerica, MA, USA), a shielded gradient system (maximum gradient strength, 630 mT/m), and a transmit/receive birdcage coil (inner diameter, 23 mm ; Bruker Corp.). Conventional spin-echo T2-weighted data were acquired with the following parameters : TR/time to echo (TE) = 3,000/21.2 milliseconds ; field of view (FOV) = 16 × 16 mm ; matrix = 160 × 160 ; slice thickness = 0.2 mm ; and acquisition time = 24 minutes. For the myocardial anisotropy evaluation, 2 volumes of pulse-field gradient spin-echo diffusion-weighted images (DWI) were acquired with the following parameters : TR/TE = 3,000/21.2 milliseconds ; FOV = 16 × 16 mm ; matrix = 160 × 160 ; slice thickness = 0.2 mm ; number of DW directions = 30 each, with a b-value of 500 s/mm^2 ; and b = 0 s/mm^2 to determine the signal-to-noise ratio. The motion probing gradient duration was 4, the interval was 11 milliseconds, and the acquisition time was 12 hours 48 minutes.

Image processing

For DTI data processing and image reconstruction, the Diffusion Toolkit software program (TrackVis.org ; Athinoula A. Martinos Center for Biomedical Imaging, Massachusetts General Hospital, Charlestown, MA, USA) was used to obtain the eigenvalues (λ1, λ2, and λ3) and FA[11]. Of these eigenvalues, λ1 represents the longitudinal diffusivity parallel to muscle fibers, λ2 represents the diffusivity perpendicular to λ1, and λ3 represents the diffusivity perpendicular to both λ1 and λ2.

The TrackVis software program (TrackVis.org) was used for fiber tracking based on the fiber assignment by a continuous tracking algorithm, which tracked the orientation of λ1 in a pixel-by-pixel manner in a 3D space.

Regions of interest

The MRI was performed at the same levels as those in the 3 histological slices used to determine the fibrosis rate. Regions of interest (ROIs) were drawn to outline the entire RV free wall ; the 3 eigenvalues and FA were measured at each of the 3 levels, and their mean values were calculated

as follows :

Mean λ1 = (1λ of slice 2+λ1 of slice 3+λ1 of slice 4)/3
Mean FA = (FA of slice 2+FA of slice 3+FA of slice 4)/3

Fibers with lengths ≤ 1 mm were excluded from the fiber tractographic analysis. The ROIs were drawn to outline the entire sagittal, coronal, and transverse sections of the RV free wall to visualize the fibers that ran within these ROIs. Subsequently, ROIs were drawn around the RV free wall on 2 coronal and 2 transverse slices, and muscle fibers that ran within both of these ROIs were visualized.

Statistical analysis

Descriptive statistics were reported with medians and interquartile ranges. Comparisons among groups were performed with the Mann–Whitney *U* test or with the Kruskal–Wallis test for more than 2 groups. Post-hoc multiple comparisons were conducted with Bonferroni's method. Spearman's correlation coefficients were calculated to assess the correlations between the RV free wall fibrosis percentage and RV free wall longitudinal strain, RV free wall λ value, RV free wall FA value, and the number of myocardial fibers. Spearman's correlation coefficient was interpreted as follows : < 0.25, none ; 0.25 to 0.50, weak ; 0.51 to 0.75, moderate ; and > 0.75, strong[12]. All statistical analyses were performed with the GraphPad Prism version 7.00 software program (GraphPad Software, La Jolla, CA, USA). In all analyses, $P < 0.05$ indicated statistical significance.

Results

Data obtained 4 weeks postprocedure

Four weeks postprocedure the whole heart weight-to-body weight ratio was significantly greater in the PAB group (5.15) than in the sham group (3.15, $P < 0.01$) (Table 1). On the basis of the RV systolic pressure-to-LV systolic pressure ratio on cardiac catheterization and echocardiography, the PAB group had a markedly elevated RVp (0.69) and an adequate RVp load (0.26, $P < 0.01$). Regarding echocardiographic variables in the PAB group, versus those in the sham group, the HR and CO were not lower ; but RVp (78 vs. 21 mm Hg, $P < 0.01$), the TV/MV ratio (1.5 vs. 1.0, $P < 0.01$), and the RV Tei index (0.21 vs. 0.10, $P < 0.01$) were significantly higher ; and TAPSE (2.0 vs. 3.0, $P < 0.01$) was significantly lower.

Fibrosis rates

Histologically determined fibrosis rates were significantly higher in the PAB group than in the sham group at the RVOT (15.8% vs. 2.2%, $P < 0.01$), for the global RV (7.3% vs. 1.9%, $P < 0.01$), and for the RV free wall (11.4% vs. 2.0%, $P < 0.01$) (Table 1). The LV and IVS fibrosis rates were similar between the groups.

To identify areas in the RV that were susceptible to fibrosis, we measured the RVOT and RV free wall fibrosis rates per slice using the method described in Fig. 2. In the PAB group the right chamber fibrosis rate was significantly higher in the basal parts (RVOT and slice 2) than in the apex (slice 4) on the basis of post-hoc multiple comparisons (Table 2, Fig. 3) (the asterisk [*] indicates significant difference vs. slice 4 [$P < 0.01$]). The fibrosis rate was highest in the RVOT, although not to a statistically significant extent, and tended within the RV to decrease through slices 2, 3, and 4 ; i.e., the basal side of the heart had higher fibrosis rates than the apical side.

2DSTE analysis

The PAB group had significantly lower global RV and RV free wall longitudinal strains than the sham group (global RV : −15.1% vs. −22.2%, $P < 0.01$; RV free wall : −12.1% vs. −22.0%, $P < 0.01$) ; however, no decreases in the RV circumferential or radial strain values were observed (Table 1). The LV circumferential and radial strains decreased significantly in the PAB group when compared to the sham group (−17.5% vs. −20.2%, $P < 0.01$; 20.6% vs. 40.8%, $P = 0.019$, respectively). Figure 4 shows the correlation between the RV free wall fibrosis rate and longitudinal strain. The RV free wall longitudinal strain value decreased significantly as the fibrosis rate increased (Spearman's $\rho = -0.42$, $P < 0.01$). For the LV, the global LV circumferential and radial strains in the PAB group were reduced (Table 1).

DTI data

The DTI images of 3 representative cases with different RV fibrosis rates (1 from the sham group with an RV fibrosis rate of 1.5% and 2 from the PAB group with RV fibrosis rates of 8.9% and 13.8%) are shown in Figure 5. The RV free wall λ and FA values were measured in all 7 cases that underwent MRI imaging, and their correlations with the RV free wall (%) are shown in Figure 6. Of these parameters,

Table 1. Summary of data obtained at 4 weeks post-procedure

	Sham (n = 10)	PAB (n = 10)	P-value
	Median (IQR)	Median (IQR)	
BW (g)	342 (333-355)	335 (323-346)	0.47
Whole heart weight/BW	3.15 (3.1-3.3)	5.15 (4.4-5.7)	<0.01
Fibrosis (%)			
RVOT	2.2 (2.0-2.3)	15.8 (13.8-18.7)	<0.01
Global RV	1.9 (1.5-2.1)	7.3 (6.5-9.7)	<0.01
RV free wall	2.0 (1.6-2.6)	11.4 (9.4-13.4)	<0.01
Global LV	3.0 (2.5-3.4)	3.9 (3.0-5.1)	0.10
LV without IVS	2.6 (2.2-3.2)	3.3 (2.0-3.6)	0.70
IVS	2.4 (2.1-2.6)	3.2 (2.1-3.7)	0.42
Cardiac catheterization			
RV systolic pressure (mm Hg)	19 (16-20)	84 (68-100)	<0.01
RV end-diastolic pressure (mm Hg)	1.7 (1.4-1.9)	5.0 (3.0-6.8)	<0.01
LV systolic pressure (mm Hg)	70 (66-72)	120 (113-130)	<0.01
LV end-diastolic pressure (mm Hg)	2.0 (2.0-2.8)	7.4 (5.3-8.2)	<0.01
RV systolic pressure/LV systolic pressure	0.26 (0.25-0.28)	0.69 (0.52-0.85)	<0.01
Echocardiography			
RVp (mm Hg)	21 (20-22)	78 (53-95)	<0.01
4Ch. RVFAC (%)	72 (67-73)	65 (57-69)	0.072
LVEF (%)	56 (52-60)	55 (54-63)	0.74
TV/MV	1.0 (1.0-1.1)	1.5 (1.0-1.6)	<0.01
TAPSE (mm)	3.0 (2.6-3.5)	2.0 (1.6-2.3)	<0.01
RV Tei index	0.10 (0.10-0.15)	0.21 (0.19-0.27)	<0.01
HR (bpm)	389 (382-402)	378 (354-392)	0.36
CO (ml/min)	129 (112-156)	119 (99-147)	0.58
2DSTE			
Longitudinal strain (%)			
Global RV	−22.0 (−22.5 to −21.0)	−15.1 (−18.1 to −12.2)	<0.01
RV free wall	−22.0 (−22.9 to −20.0)	−12.1 (−13.9 to −10.5)	<0.01
Global LV	−18.2 (−19.0 to −16.9)	−16.3 (−19.0 to −14.8)	0.31
LV without IVS	−17.7 (−20.4 to −16.1)	−15.4 (−17.7 to −15.7)	0.075
Circumferential strain (%)			
Global RV	−15.6 (−18.5 to −13.2)	−16.8 (−17.7 to −15.7)	0.36
RV free wall	−13.4 (−15.3 to −9.0)	−15.4 (−16.9 to −14.4)	0.12
Global LV	−20.2 (−22.2 to −19.0)	−17.5 (−19.2 to −16.6)	0.010
LV without IVS	−22.2 (−23.7 to −18.0)	−18.3 (−18.9 to −15.1)	0.022
Radial strain (%)			
Global RV	17.0 (13.5-24.3)	19.3 (13.1-29.0)	0.85
RV free wall	14.7 (12.7-20.2)	18.8 (12.2-31.7)	0.49
Global LV	40.8 (27.9-46.6)	20.6 (18.6-33.4)	0.019
LV without IVS	24.9 (21.0-32.6)	36.1 (14.6-39.4)	0.97

PAB, pulmonary artery banding ; IQR, interquartile range ; BW, body weight ; RVOT, right ventricular outflow tract ; RV, right ventricle ; LV, left ventricle ; IVS, interventricular septum ; RVp, right ventricular pressure ; LVp, left ventricular pressure ; 4Ch. RVFAC, right ventricular fractional area in the 4-chamber view ; LVEF, left ventricular ejection fraction ; TV, tricuspid valve ; MV, mitral valve ; TAPSE, tricuspid annular plane systolic excursion ; HR, heart rate ; CO cardiac output ; 2DSTE, two-dimensional Speckle tracking.

Table 2. Fibrosis rate for each slice

	Sham (n = 10)	PAB (n = 10)
Fibrosis (%)	Median (IQR)	Median (IQR)
RVOT	2.4 (2.1–2.7)	15.9 (13.8–20.2)
Slice 2	2.3 (2.1–2.5)	15.7 (13.2–17.1)
Slice 3	1.7 (1.4–1.7)	11.4 (8.0–14.6)
Slice 4	1.9 (1.5–2.2)	6.4 (3.8–9.4)

PAB, pulmonary artery banding ; IQR, interquartile range ; RVOT, right ventricular outflow tract.

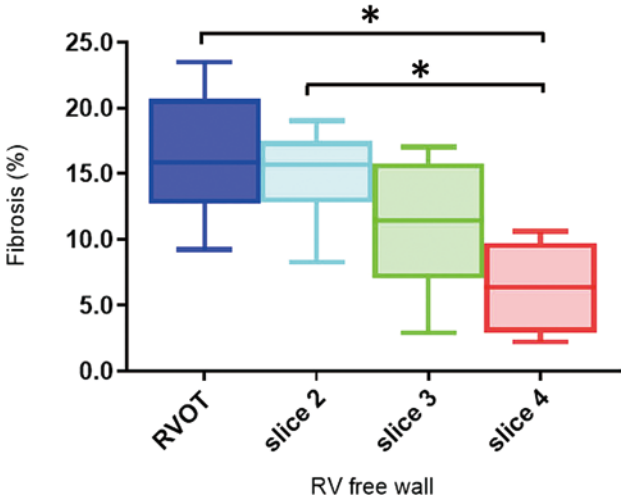

Fig. 3. Fibrosis rates (%) in the RV free wall in the PAB rats (n = 10).
Box plots showing the RV free wall in the subgroups of the PAB rats (n = 10). The lower half of the box plot depicts the 25th percentile ; the upper half of the box plot, the 75th percentile ; the horizontal line dividing the upper and lower halves of the box plot, the median ; the upper whisker, the maximum ; and the lower whisker, the minimum. Significant differences ($P < 0.01$) between groups are indicated by arrows and asterisks (*). The fibrosis rate was higher in the basal parts (RVOT and slice 2) than in the apex (slice 4). PAB, pulmonary artery banding ; RVOT, right ventricular outflow tract ; RV, right ventricle.

λ1 was significantly negatively correlated with RV free wall fibrosis (% ; Spearman's $\rho = -0.79$, $P = 0.036$).

The tractography data and images were obtained. First, the myocardium that only passed through the RV free wall was depicted in sagittal, coronal, and transverse sections ; the number of myocardial fibers was reduced in all sections in the PAB group compared to the sham group (Table 3). Three representative tractography images similar to those in Figure 5 are shown in Figure 7 (a, b, c). The number of myocardial fibers per voxel is shown because the area of the RV free wall differs from that of RV hypertrophy, and greater RV hypertrophy is associated with a larger RV area. As fibrosis increased, the number of myocardial fibers decreased in the sagittal, coronal, and transverse sections. The numbers of myocardial fibers in both the coronal and transverse sections were reduced in the PAB group compared to the sham group (Table 4, Fig. 8). The distance between 2 sagittal cross-sections was not determined in this study due to the difficulty in equalizing the distance between the sham and PAB groups.

Discussion

This study demonstrated that DTI and 2DSTE may predict and locally diagnose RV myocardial fibrosis, which is a compensatory change after chronic pressure loading. Furthermore, DTI allows for successful 3D visualization of RV myocardial fibrosis.

Late gadolinium-enhanced cardiac MRI has been used for evaluating myocardial fibrosis[13]. However, while this method is superior for evaluating myocardial tissue, it cannot detect diffuse fibrosis. Importantly, use of contrast agent is often discouraged in cardiac disease cases, especially in infants. Therefore, we focused on DTI, which is minimally invasive and requires no contrast medium, and fibrosis severity quantification in specific regions that allowed for objective fibrosis staging. We used ex vivo DTI due to difficulties in synchronizing the rats' fast HRs and body movements. Moreover, the ex vivo analysis allowed for the entire RV fibrosis measurement rather than a single section measurement. Few reports have compared in vivo and ex vivo DTI parameters. In a brain MRI study, Guilfoyle et al. and Haga et al. reported that in and ex vivo anisotropy were comparable[14,15]. Thus, we considered our study results comparable to in vivo study results.

Here, among the DTI indices, 1 showed a significant negative correlation with RV myocardial fibrosis. This was consistent with the 2DSTE results, where RV longitudinal strain was most closely correlated with RV myocardial fibrosis. RV myocardium is arranged in 2 layers : longitudinal and ring-shaped muscles on the endocardial and epicardial sides, respectively, with the predominant fibers being longitudinal. RV myocardial fibrosis may disrupt the myocardial alignment of the longitudinal muscle, resulting in decreased RV longitudinal strain and λ1 on echocardiography and MRI,

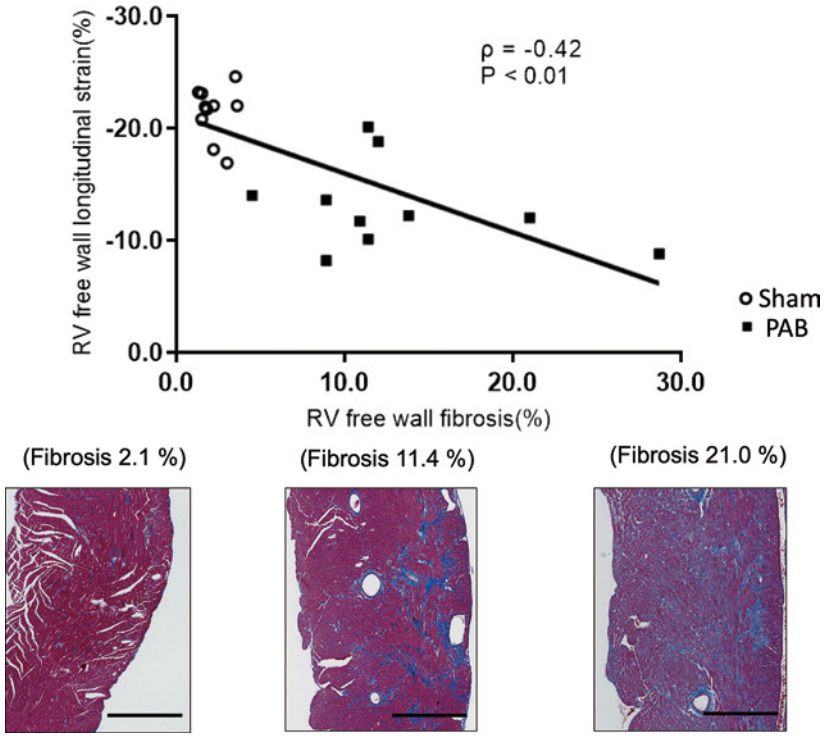

Fig. 4. Correlation between fibrosis (%) and longitudinal strain in the RV free wall. The figure shows the correlation between the fibrosis (%) and longitudinal strain in the RV free wall. Examples of trichrome-stained RV free wall regions with different degrees of fibrosis are shown (blue). A significant negative correlation was observed between the RV longitudinal strain score and fibrosis (Spearman's $\rho = -0.42$, $P < 0.01$). Thus, the RV longitudinal strain decreased as the fibrosis rate increased. Scale bar = 1 mm. RV, right ventricle.

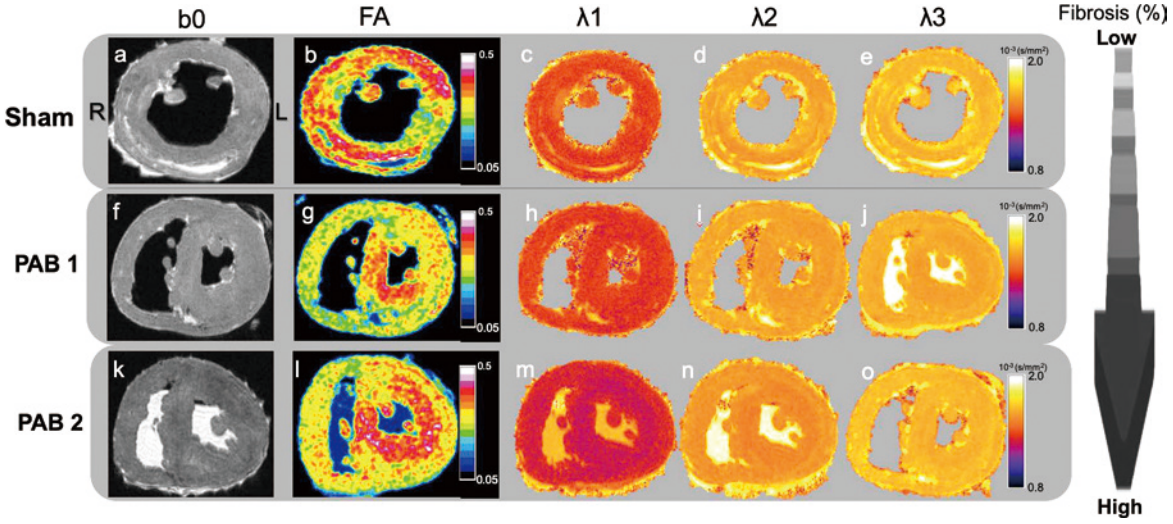

Fig. 5. Representative DTI images in the transverse plane.
The image source is an MRI. (a, f, k) b0 images (no diffusion encoding). (b, g, l) FA maps. (c-e, h-j, m-o) λ maps of the heart from a rat in the sham group (top panels : this rat had a histologically determined RV fibrosis rate of 1.5%) and from rats in the PAB group (middle and bottom panels : fibrosis rates of 8.9% and 13.8%, respectively). R, right ; L, left. DTI, diffusion tensor imaging ; MRI, magnetic resonance imaging ; FA, fractional anisotropy ; PAB, pulmonary artery banding.

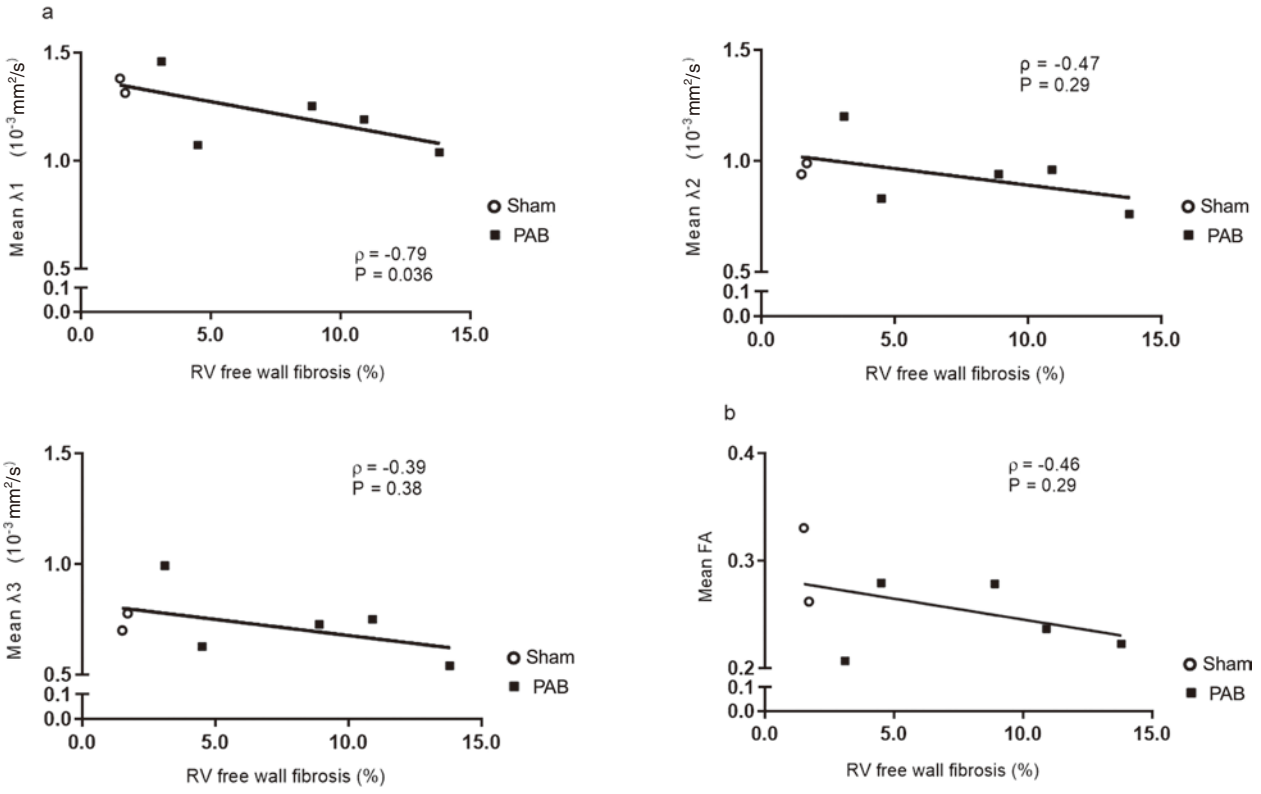

Fig. 6. Correlation between fibrosis of the RV free wall and DTI parameters.
Among the DTI parameters, only λ1 showed a significant negative correlation with fibrosis of the RV free wall. DTI, diffusion tensor imaging ; RV, right ventricle.

Table 3. Number of myocardial fibers only passing through the RV free wall

	Sham (n = 2)	**PAB (n = 5)**
No. of fibers/voxel	Median (IQR)	Median (IQR)
Sagittal	10.2 (9.9–10.5)	7.2 (3.7–8.4)
Coronal	24.8 (23.0–26.5)	15.3 (10.1–15.7)
Transverse	19.3 (18.9–19.8)	8.6 (4.6–12.9)

Sagittal, coronal, and transverse sections all showed fewer myocardial fibers in the PAB group compared to the sham group. PAB, pulmonary artery banding ; IQR, interquartile range.

respectively. Additionally, RV fibrosis was stronger on the basal side of the heart than the apical. Weidemann et al. reported strong LV myocardial fibrosis on the basal and endocardial sides of the LV in patients with severe aortic valve stenosis[16]. Here, the PAB group was based on a chronic pressure loading model, in which the degree of PA strangulation gradually increased with weight gain, resulting in a gradual increase in RVp[17]. As in the LVs of severe aortic stenosis patients, fibrosis may have been more severe in the RV on the basal side of the heart due to its proximity to the pressure load source.

We also attempted to visualize myocardial fibrosis using fiber tractography. When evaluating myocardial fibrosis, Sosnovik et al. used a more detailed fiber tractography technique, with the 515 axis as the diffusion axis[18]. However, myocardial fibrosis has fewer cross-fibers than cerebral nerves and a higher pixel resolution was considered to avoid normal and fibrotic tissue mixing. Thus, here, the 400 μm resolution set by Sosnovik et al. was 100 μm[18]. Moreover, we set 12 diffusion axes, which were applicable in children, and successfully constructed a 3D myocardial arrangement of a fibrotic heart using fiber tractography. Consequently, we successfully constructed a 3D myocardial sequence in any region using red, green, and blue lines. We found that the depicted number of myocardial fibers decreased with fibrosis. Myocardial RV free wall alignment was continuous in the sham group, whereas myocardial alignment continuity in the RV free wall sagittal, coronal, and transverse planes was not observed in the PAB group,

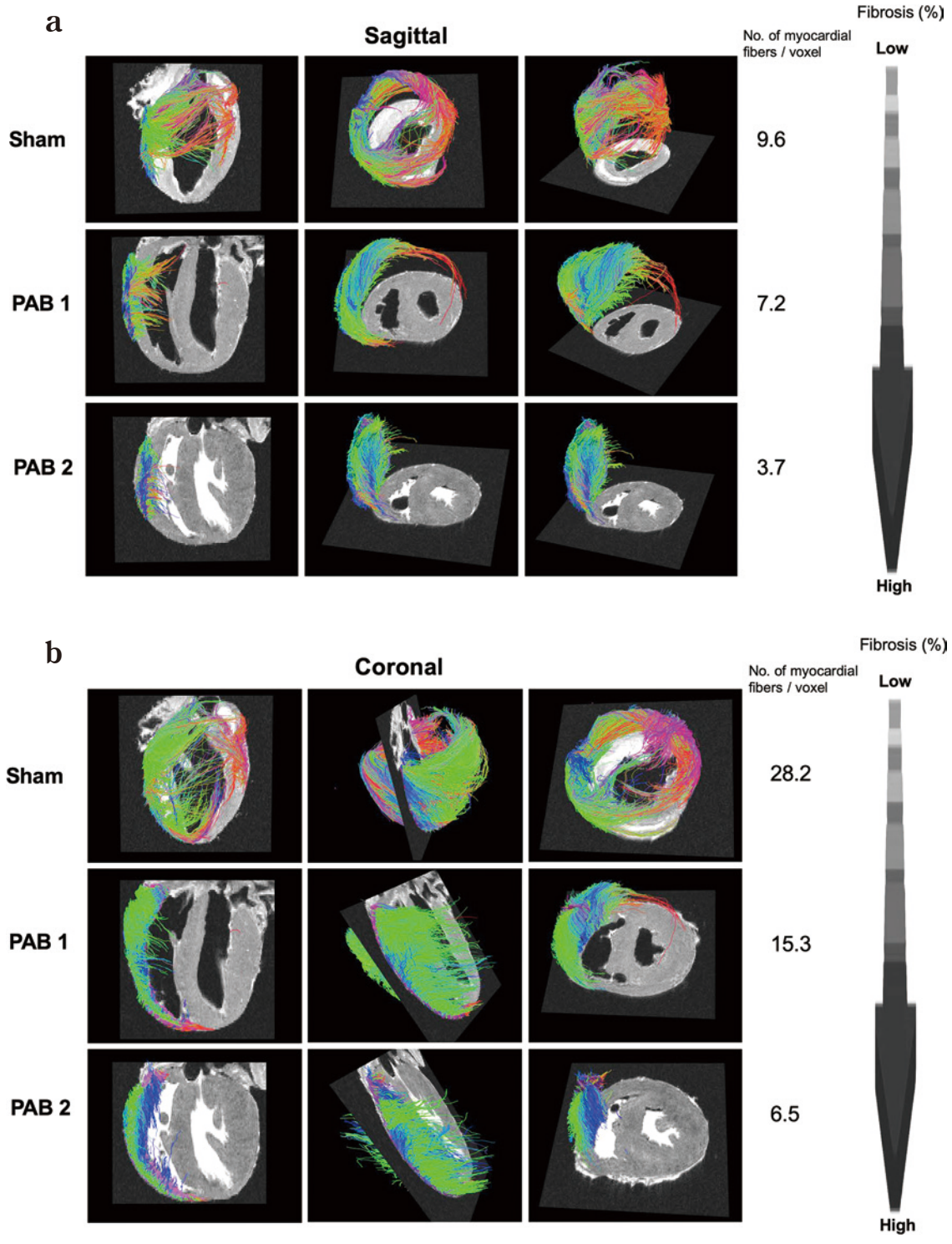

and the number of myocardial fibers was significantly reduced. Coronal and transverse sections showed myocardial fibers passing through both planes at the same distance, and, visually, the decrease in the number of myocardial fibers was more pronounced with an increased fibrosis rate. Thus, the number of myocardial fibers may be a useful measure.

Here, a decrease in RV longitudinal strain, which oc-

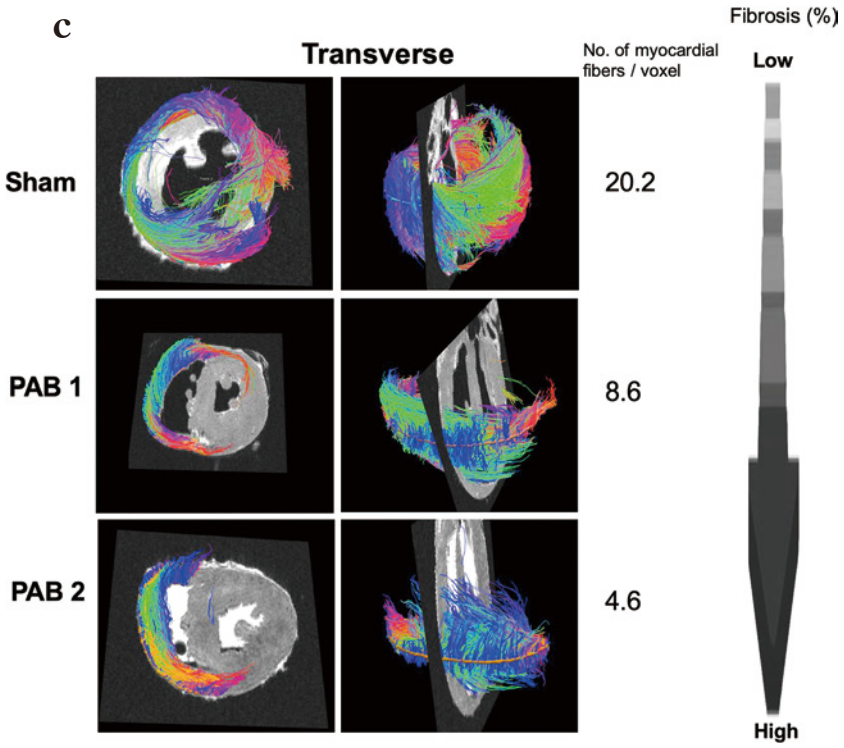

Fig. 7. Representative fiber tractography images in sagittal (a), coronal (b), and transverse (c) planes. The source of image is an MRI. Myocardial fibers passing through the RV free wall are visualized using the same 3 hearts shown in Figure 5. Compared with the sham rats, PAB rats had fewer myocardial fibers per voxel in all planes. Red, transverse fibers ; green, anteroposterior fibers ; blue, craniocaudal fibers. MRI, magnetic resonance imaging ; RV, right ventricle ; PAB, pulmonary artery banding.

curred earlier than the decrease in RVFAC (a conventional measure of echocardiographic contractility), was observed on 2DSTE. This was consistent with Coppola et al.'s findings[19] Interestingly, left ventricular circumferential and radial strain also decreased. There are multiple reports of LV STEs in patients with LV lesions[20-22]. Similarly, studies of RV strain values in patients with RV lesions are numerous[23,24]. However, to our knowledge, our study is the first to report that LV circumferential and radial strain preceded a decrease in LV longitudinal strain in RV pressure-overloaded hearts. Importantly, in this study, the LV itself did not have any fibrosis or functional problems, possibly due to the RVp load pressurized the IVS, which affected LV function. We believe that the depressurization direction in the IVS is on the short-axis ; therefore, LV global longitudinal strain did not decrease, whereas the LV global and circumferential strain did.

This study had limitations. First, this was a single center study with a small sample size. Furthermore, we cannot rule out that sedation may have affected the hemodynamic assessments. Therefore, extrapolation of these results onto humans may be difficult. However, since we used an animal model with little inter-individual bias, the tests' internal validity and results' robustness were ensured. We plan to increase the case numbers to examine the reproducibility of these results. Second, the 4-week observation period may not be optimal for early RV dysfunction assessment. However, when the rats were observed for more than 4 weeks in the PAB model, many died due to decreased overall cardiac contractility, which included the LV. Moreover, because a decrease in the strain on 2DSTE is considered an earlier indicator of reduced cardiac function than in the EF[17], we believe that the 4-week observation period may reasonably reflect early RV dysfunction. Third, DTI requires a significant amount of time. However, recently there has been extensive research into compressed sensing[25] and multi-band methods[26,27] that may reduce the imaging time. These innovations should contribute to the development and clinical application of cardiac MRI. When these problems are overcome and application in pediatric patients becomes possible,

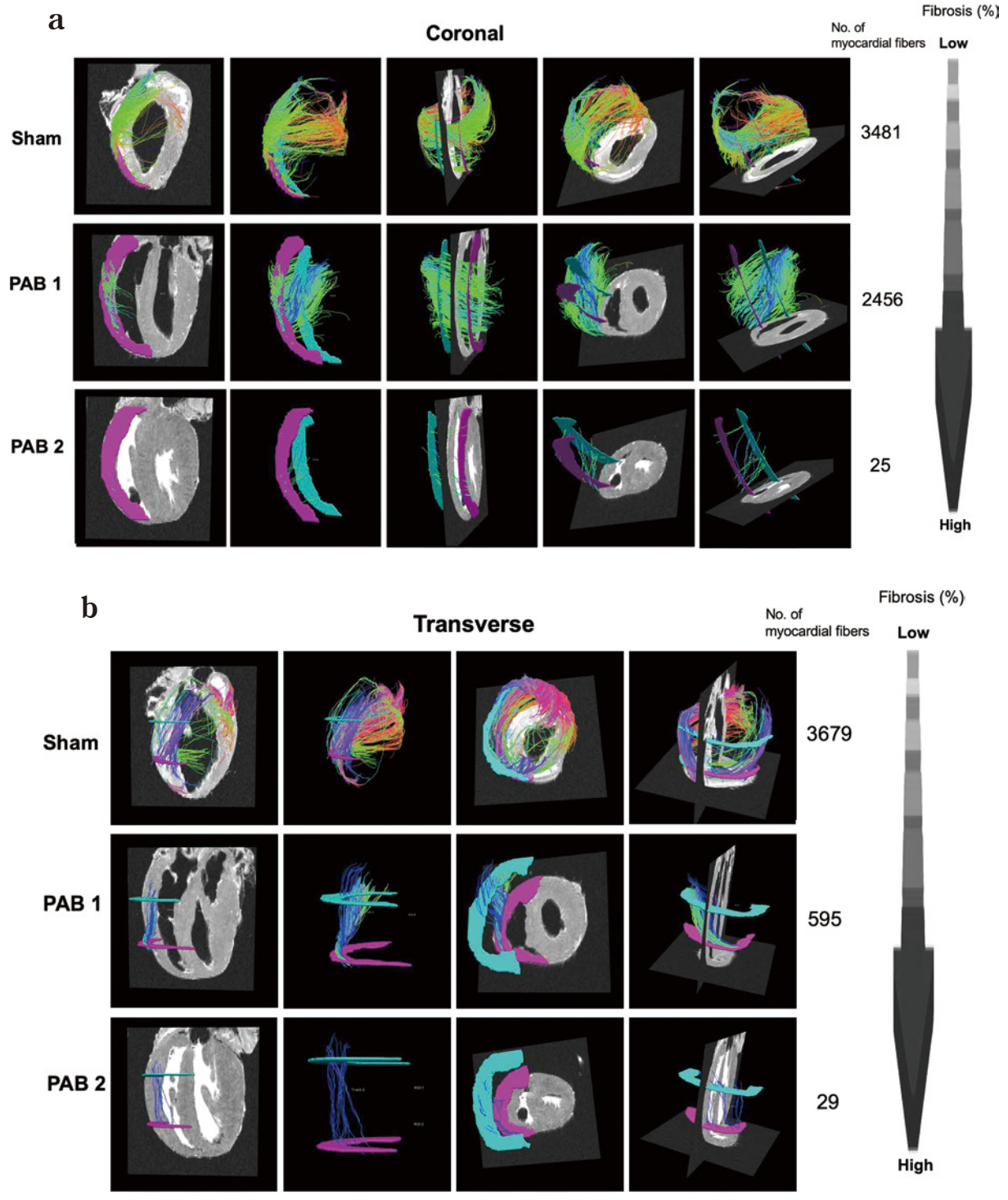

Fig. 8. Myocardial fibers running through the 2 RV free wall levels based on fiber tractography.
The image source is an MRI. (a) Coronal. (b) Transverse. The same specimens as shown in Figures 5 and 7 were used. Fibers passing through the 2 levels (in light blue and purple) are visualized. The PAB group had fewer fibers running these distances than the sham group. MRI, magnetic resonance imaging ; RV, right ventricle ; PAB, pulmonary artery banding.

Table 4. Number of myocardial fibers passing between the two RV free wall levels

	Sham (n = 2)	**PAB (n = 5)**
No. of fibers	Median (IQR)	Median (IQR)
Coronal	3,065 (2,857–3,481)	2,456 (106–2,559)
Transverse	3,026 (2,700–3,679)	595 (127–1,283)

The numbers of myocardial fibers were lower in the PAB group than in the sham group in both the coronal and transverse sections. PAB, pulmonary artery banding ; IQR, interquartile range.

this study will contribute to DTI parameter interpretation in pediatric patients.

Conclusions

In this study, we suggested that 2DSTE and DTI could predict RV myocardial fibrosis in a rat model of chronic RVp-loaded rats subjected to PAB.

Authors have no conflict of interest.

References

1. Kaul S, Tei C, Hopkins JM, Shah PM. Assessment of right ventricular function using two-dimensional echocardiography. Am Heart J. 1984 ; 107 : 526–31.
2. Meluzin J, Spinarova L, Bakala J, Toman J, Krejci J, Hude P, et al. Pulsed Doppler tissue imaging of the velocity of tricuspid annular systolic motion ; a new, rapid, and non-invasive method of evaluating right ventricular systolic function. Eur Heart J. 2001 ; 22 : 340–8.
3. Tei C, Dujardin KS, Hodge DO, Bailey KR, McGoon MD, Tajik AJ, et al. Doppler echocardiographic index for assessment of global right ventricular function. J Am Soc Echocardiogr. 1996 ; 9 : 838–47.
4. Meris A, Faletra F, Conca C, Klersy C, Regoli F, Klimusina J, et al. Timing and magnitude of regional right ventricular function : a speckle tracking-derived strain study of normal subjects and patients with right ventricular dysfunction. J Am Soc Echocardiogr. 2010 ; 23 : 823–31.
5. Pedrinelli R, Canale ML, Giannini C, Talini E, Dell'Omo G, Di Bello V. Abnormal right ventricular mechanics in early systemic hypertension : a two-dimensional strain imaging study. Eur J Echocardiogr. 2010 ; 11 : 738–42.
6. Verhaert D, Mullens W, Borowski A, Popovic ZB, Curtin RJ, Thomas JD, et al. Right ventricular response to intensive medical therapy in advanced decompensated heart failure. Circ Heart Fail. 2010 ; 3 : 340–6.
7. Zhang J, Aggarwal M, Mori S. Structural insights into the rodent CNS via diffusion tensor imaging. Trends Neurosci. 2012 ; 35 : 412–21.
8. Chen J, Song SK, Liu W, McLean M, Allen JS, Tan J, et al. Remodeling of cardiac fiber structure after infarction in rats quantified with diffusion tensor MRI. Am J Physiol Heart Circ Physiol. 2003 ; 285 : H946–54.
9. Tseng WY, Dou J, Reese TG, Wedeen VJ. Imaging myocardial fiber disarray and intramural strain hypokinesis in hypertrophic cardiomyopathy with MRI. J Magn Reson Imaging. 2006 ; 23 : 1–8.
10. Wu EX, Wu Y, Nicholls JM, Wang J, Liao S, Zhu S, et al. MR diffusion tensor imaging study of postinfarct myocardium structural remodeling in a porcine model. Magn Reson Med. 2007 ; 58 : 687–95.
11. Mori S, van Zijl PC. Fiber tracking : principles and strategies — a technical review. NMR Biomed. 2002 ; 15 : 468–80.
12. Dawson B, Trapp RG. Basic and Clinical Biostatistics. 4th Ed. New York : Lange Medical Books/McGraw-Hill ; 2004.
13. Hoffmann R, Altiok E, Friedman Z, Becker M, Frick M. Myocardial deformation imaging by two-dimensional speckle-tracking echocardiography in comparison to late gadolinium enhancement cardiac magnetic resonance for analysis of myocardial fibrosis in severe aortic stenosis. Am J Cardiol. 2014 ; 114 : 1083–8.
14. Guilfoyle DN, Helpern JA, Lim KO. Diffusion tensor imaging in fixed brain tissue at 7.0 T. NMR Biomed. 2003 ; 16 : 77–81.
15. Haga Y, Hata J, Uematsu A, Seki F, Komaki Y, Mizumura M, et al. MR imaging properties of ex vivo common marmoset brain after formaldehyde fixation. Magn Reson Med Sci. 2019 ; 18 : 253–9.
16. Weidemann F, Herrmann S, Stork S, Niemann M, Frantz S, Lange V, et al. Impact of myocardial fibrosis in patients with symptomatic severe aortic stenosis. Circulation. 2009 ; 120 : 577–84.
17. Fujimoto Y, Urashima T, Shimura D, Ito R, Kawachi S, Kajimura I, et al. Low cardiac output leads hepatic fibrosis in right heart failure model rats. PLoS One. 2016 ; 11 : e0148666.
18. Sosnovik DE, Wang R, Dai G, Wang T, Aikawa E, Novikov M, et al. Diffusion spectrum MRI tractography reveals the presence of a complex network of residual myofibers in infarcted myocardium. Circ Cardiovasc Imaging. 2009 ; 2 : 206–12.
19. Coppola C, Riccio G, Barbieri A, Monti MG, Piscopo G, Rea D, et al. Antineoplastic-related cardiotoxicity, morphofunctional aspects in a murine model : contribution of the new tool 2D-speckle tracking. Onco Targets Ther. 2016 ; 9 : 6785–94.
20. Carstensen HG, Larsen LH, Hassager C, Kofoed KF, Jensen JS, Mogelvang R. Basal longitudinal strain predicts future aortic valve replacement in asymptomatic patients with aortic stenosis. Eur Heart J Cardiovasc Imaging. 2016 ; 17 : 283–92.
21. Cameli M, Mondillo S, Righini FM, Lisi M, Dokollari A, Lindqvist P, et al. Left ventricular deformation and myocardial fibrosis in patients with advanced heart failure requiring transplantation. J Card Fail. 2016 ; 22 : 901–7.
22. Dusenbery SM, Lunze FI, Jerosch-Herold M, Geva T, New-

burger JW, Colan SD, et al. Left ventricular strain and myocardial fibrosis in congenital aortic stenosis. Am J Cardiol. 2015 ; 116 : 1257-62.
23. Lisi M, Cameli M, Righini FM, Malandrino A, Tacchini D, Focardi M, et al. RV longitudinal deformation correlates with myocardial fibrosis in patients with end-stage heart failure. JACC Cardiovasc Imaging. 2015 ; 8 : 514-22.
24. Lu KJ, Chen JX, Profitis K, Kearney LG, DeSilva D, Smith G, et al. Right ventricular global longitudinal strain is an independent predictor of right ventricular function : a multimodality study of cardiac MRI, real time 3-dimensional echocardiography and speckle tracking echocardiography. Echocardiography. 2015 ; 32 : 966-74.
25. Lustig M, Donoho D, Pauly JM. Sparse MRI : The application of compressed sensing for rapid MR imaging. Magn Reson Med. 2007 ; 58(6) : 1182-95. Epub 2007/10/31. doi : 10.1002/mrm.21391. PubMed PMID : 17969013.
26. Setsompop K, Gagoski BA, Polimeni JR, Witzel T, Wedeen VJ, Wald LL. Blipped-controlled aliasing in parallel imaging for simultaneous multislice echo planar imaging with reduced g-factor penalty. Magn Reson Med. 2012 ; 67(5) : 1210-24. Epub 2011/08/23. doi : 10.1002/mrm.23097. PubMed PMID : 21858868 ; PubMed Central PMCID : PMCPMC3323676.
27. Ugurbil K, Xu J, Auerbach EJ, Moeller S, Vu AT, Duarte-Carvajalino JM, et al. Pushing spatial and temporal resolution for functional and diffusion MRI in the Human Connectome Project. Neuroimage. 2013 ; 80 : 80-104. Epub 2013/05/25. doi : 10.1016/j.neuroimage.2013.05.012. PubMed PMID : 23702417 ; PubMed Central PMCID : PMCPMC3740184.